

Synthesis, Characterization And Wear Behavior Of Co_{0.5} Cr Cu_{0.5} Fe Ni_{1.5} Al Ti_{0.4} And Co Cr Fe Ni Al_{0.25} Ti_{0.75} High Entropy Alloy (Hea) Prepared By Mechanical Alloying

Surendra kumar verma¹, Prof. krishna bhushan patel²

^{1,2}Dept of ME

^{1,2}RGPM, Bhopal

Abstract- Structure-tribological property relations have been studied for two high entropy alloys (HEAs). Microhardness, room temperature sliding friction coefficients and wear rates were determined for two HEAs: Co_{0.5}CrCu_{0.5}Fe Ni_{1.5}AlTi_{0.4} and Co Cr Fe Ni Al_{0.25} Ti_{0.75}. Wear surfaces were characterized with scanning electron microscopy and micro-Raman spectroscopy to determine the wear mechanisms and tribochemical phases, respectively. It was determined that the both HEAs exhibit an excellent balance of high hardness and lower wear rates compared to 440C stainless steel, a currently used bearing steel. This was attributed to their more ductile body centered cubic (BCC) solid solution phase along with the formation of tribochemical Cr oxide and Ti oxide phases, respectively, in the wear surfaces. This study provides guidelines for fabricating novel, low-friction, and wear-resistant HEAs for potential use at room and elevated temperatures, which will help reduce energy and material losses in friction and wear applications.

I. INTRODUCTION

HEAs can be defined as an alloy that consists of at least five principal elements having atomic percentages between 5% and up to 35% in equiatomic or near-equiatomic ratios as well as minor elements [8]. HEAs were first explored by Cantor et al. and Yeh et al. independently. Since 1995, they named this new type of alloys as High Entropy Alloys since the configurational entropy is a maximum when the elements are in equimolar ratios and this entropy contributes to lowering Gibbs free energy, which helps stabilize the solid solution phase [9]. More recently, HEAs have also been referred to as complex concentrated alloys (CCAs)

Recently, high entropy alloys (HEAs) consisting of multiple principal elements have attracted wide interest due to their novel microstructures and properties [1]. Many research groups have been investigating these new class of metallic alloys that have potential for many industrial and engineering

applications. Studies conducted on HEAs have revealed that such alloys exhibit increased strength and hardness, oxidation resistance, and stability at higher temperatures. Such improvements in properties and characteristics give HEAs a very important potential role in a wide range of engineering applications, such as molds, tools, gears, bearings, etc. [2].

The multi-component equi-molar alloys should be located at the center of a multi-component phase diagram, and their Configurational entropy of mixing reaches its maximum for a solution phase. These alloys are defined as HEAs by Yeh et al. [1], and named by Cantor et al. [3] as multi-component alloys. Both refer to essentially the same concept. These systems have been given some other names, such as multi-principal-element alloys, equi-molar alloys, equi-atomic ratio alloys, substitutional alloys, and multi-component alloys. Cantor et al. [3] has concluded that the conventional alloy development method leads to a huge amount of knowledge about alloys based on one or two components, but very scarce knowledge about alloys containing several main components in near-equal proportions. Theoretical and experimental works on the existence, structure, and properties of crystalline and solid solution phases have been restricted to alloys based on one or two main components [5]. Thus, the information, understanding, and applications are highly developed on alloys close to the corners and edges of a multi-component phase diagram, with much less knowledge, to the extent of ignorance, about possible alloys located at the center of the phase diagram. This imbalance is significant for ternary alloys and becomes rapidly much more pronounced as the number of components increases. For most quaternary and other higher-order systems, information about alloys at the center of the phase diagram is virtually nonexistent except those HEA systems that have been reported very recently [6].

II. EXPERIMENTAL PROCEDURES AND METHODS

Composition of Pre-Mixed Powder

- Non-equiatomic elemental blends of following powders of high purity (greater than 95% for Iron and 99% for other powders).
- The total weight of each pre-alloy powder blend was 20 g.
- The aim was to synthesize the system $\text{Co}_{0.5} \text{Cr Cu}_{0.5} \text{Fe Ni}_{1.5} \text{Al Ti}_{0.4}$ and $\text{Co Cr Fe Ni Al}_{0.25} \text{Ti}_{0.75}$ via mechanical alloying.

Table1: Weightwise composition of the four pre-alloy powder blends

Specimens Name	Composition Notation
Alloy 1	$\text{Co}_{0.5} \text{Cr Cu}_{0.5} \text{Fe Ni}_{1.5} \text{Al Ti}_{0.4}$
Alloy 2	$\text{Co Cr Fe Ni Al}_{0.25} \text{Ti}_{0.75}$

Mechanical Alloying: Done in Fritsch Pulverisette 5 planetary ball mill, using high chrome steel vials lined with tungsten carbide. ball-to-powder weight ratio of 10:1 using tungsten carbide balls as grinding media, of 10 mm diameter. The PCA (Process Controlling Agent) was 50 ml 2-propanol for each batch of 20 g powder. PCA was used to prevent agglomeration of powder and deposition on the enclosure walls and the balls used for grinding total time for milling was 16 hours for each batch. The alloyed powders were then stored in airtight eppendorf @ centrifuge tubes, before compaction process for further evaluation.

Compaction: The milled powders were consolidated using a hydraulic press and high chrome steel die, punch, plunger apparatus lined with tungsten carbide. uniaxial pressure of 600 MPa for 60 seconds to form cylindrical pellets. Dimensions of each pellet: width = 2.85 mm and diameter = 12.40 mm.. Weight of each compressed batch of powder was 1.5 g, with two samples made from each alloy composition.

Sintering: Sintering of compacted pellets was done in Microprocessor Controlled, open top type Furnace. Temperature of sintering was 800°C continuously for about 300 minutes. The pellets were sintered with an initial temperature of 300K of furnace (room temperature) at a heating rate of 10 degree centigrade per minute. The pellets were then allowed to cool inside the furnace to room temperature at a negative rate of 0.5 degree centigrade per minute. Thin layer of oxide was found to be formed on the surface of each pellet. This could be possibly due to sintering in an open atmosphere.

Characterization: Optical Microscopy, Scanning Electron Microscopy, X-Ray Diffraction, Vickers Microhardness, Wear analysis

III. RESULTS AND DISCUSSION

XRD and Microstructure Analyses

Alloy 1- $\text{Co}_{0.5} \text{CrCu}_{0.5} \text{FeNi}_{1.5} \text{AlTi}_{0.4}$

The alloy $\text{Co}_{0.5} \text{CrCu}_{0.5} \text{FeNi}_{1.5} \text{AlTi}_{0.4}$ high entropy alloy was prepared by mechanical alloying through ball milling. The XRD pattern shown in Figure 1 shows that the alloy consists of two ordered and disordered BCC phases with FCC phase of Cu-rich region. Figure 2 shows an SEM micrograph of the alloy. It has been reported that this HEA exhibits lamellar-like morphologies consisting of white and dark areas with white contrast for ordered Heusler L21 phase, referred to as (α) that with Cu-rich precipitates, and darker contrast attributed to disordered (β) BCC phase. The chemical composition listed in Table 2 discloses that ordered L21 phase is rich in Al, Ti, and Ni. Whereas, the disordered β phase is rich in Fe and Cr[1]. In the literature about such an alloy, F.J. Wang et al.[2] pointed out that the $\text{Ti}_{0.5} \text{CrFeCoNiAlxCu}_{1-x}$ high entropy alloy possesses two BCC phases when the Al content is higher than 0.7, which is consistent with what was found by D. Choudhuri et al. In addition, X.W. Qiu reported the existence of two BCC phases with Laves intermetallic compound [3]. Moreover, Yu-Liang Chena stated that as-cast $\text{Cu}_{0.5} \text{NiAlCoCrFeTi}$ high entropy alloy consists of two BCC phases with small peaks correspond to an FCC phase [4,9,18]. the calculated VEC value for alloy 1 is 7.38, which means the alloy should contain mixed BCC and FCC according to Guo's proposal [5,19,28], and this is consistent with the finding of Choudhuri et al.

Table 2. Chemical composition in at. % of phases present in alloy 1 [1].

phase	Ni	Al	Ti	Fe	Cr	Co	Cu
B	4.0	0.4	1.3	37.5	46.3	8.9	0.5
L21(α)	48.8	13.4	10.5	8.9	0.9	12.4	5.1
Cu-precipitate	5.2	3.8	0.3	0.3	0.2	1.2	89

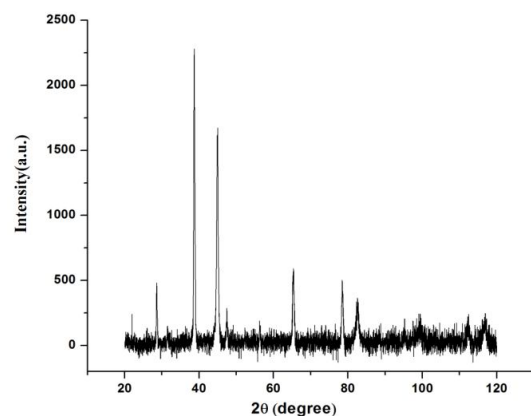


Figure 1. XRD pattern of $\text{Co}_{0.5} \text{CrCu}_{0.5} \text{FeNi}_{1.5} \text{AlTi}_{0.4}$ high entropy alloy 1

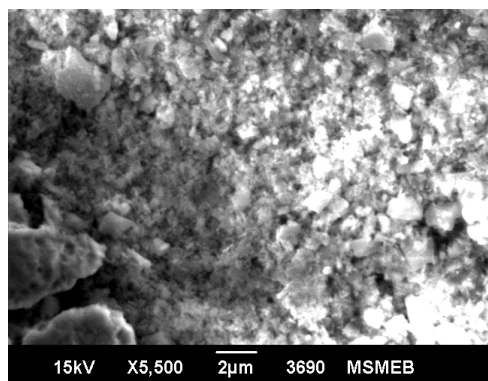
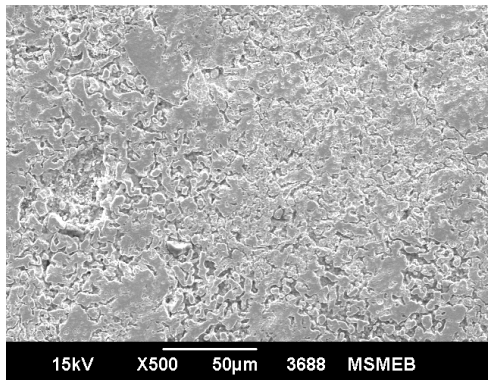


Figure 2. Representative SEM image of Co_{0.5}CrCu_{0.5}FeNi_{1.5}AlTi_{0.4} high entropy alloy

Table 3 Presents the chemical compositions in at. % of the phases present in alloy 2.

Phase	Al	Ti	Cr	Fe	Co	Ni
Dark	22.04	18.14	6.27	8.90	22.25	22.40
Gray	9.46	16.98	12.36	15.94	22.36	22.90
White	2.01	15.07	21.37	22.62	22.41	16.52

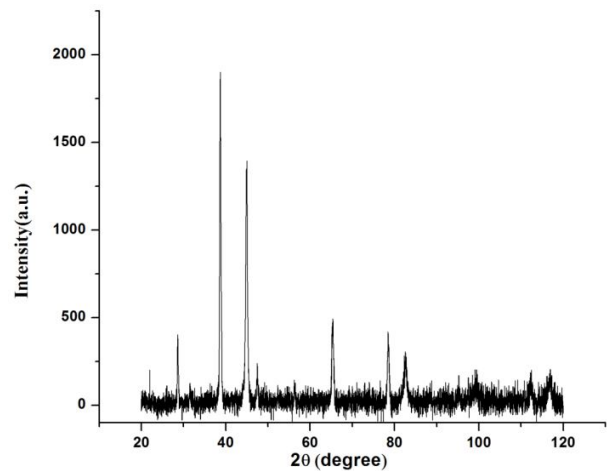


Figure 3. XRD pattern of CoCrFeNiAl_{0.25}Ti_{0.75} high entropy alloy 2.

Alloy 2 – CoCrFeNiAl_{0.25}Ti_{0.75} The XRD pattern given in Figure 3 shows set of peaks for two BCC phases referred to as 1 and 2, ordered BCC, FCC, and a large lattice constant intermetallic compound which is likely either a σ or χ phase. Figure 4 presents the back scattered SEM micrographs of CoCr Fe Ni Al_{0.25} Ti_{0.75} high entropy alloy. It consists of three contrasted regions, namely dark, white, and gray. Table 3 shows that the dark region indicates the presence BCC, and this region is rich in Ti, Ni and Al. It is possible this is L21 phase, as in HEA 1. In addition, the white region is rich in Fe and Cr, and is likely a

σ or χ phase (with larger lattice parameter) that are common in Fe-Cr steels. Moreover, BCC and FCC phases are embedded in these regions as well. Whereas the grayish region consists of BCC matrix composed of irregular and needle-like morphologies having BCC crystal structure. Zhang et al.[6] reported that CoCrFeNiTiAl_x (x= 0.5) high-entropy alloy consists of FeCr-based BCC and NiAl-based BCC solid solutions with CoTi and FeTi as minor phases. Moreover, it was stated that CoCrFeNiTiAl_x high-entropy alloy contains two BCC solid solutions with a Laves phase determined as FeTi type[7]. the calculated VEC value for alloy 2 is 7.35, which means the alloy should contain mixed BCC and FCC according to Guo’s proposal [5], and this is consistent with XRD findings.

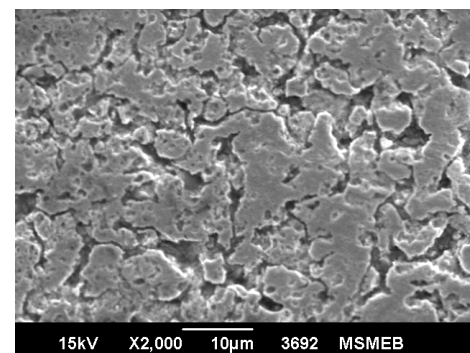
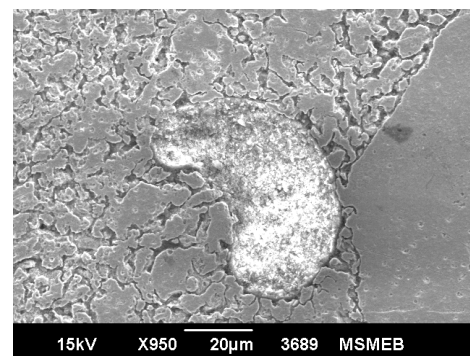


Figure 4. SEM images of CoCrFeNiAl_{0.25}Ti_{0.75} high entropy alloy showing the different regions.

IV. MICROHARDNESS ANALYSIS

Alloy 1:

The hardness distribution Profiles of Alloy 1 ($\text{Co}_{0.5}\text{CrCu}_{0.5}\text{FeNi}_{1.5}\text{AlTi}_{0.4}$) is shown in Figure 5 The hardness distribution curves show three regions, corresponding to the sample area of the highest hardness area, medium hardness zone, and the lower hardness area, respectively. The surface microhardness of Alloy 1 is up to $626 \pm 10\text{HV}$. The likely reasons behind the increase can be attributed to the Ti content, which is greater than 0.4, and has been reported to increase the surface microhardness because of the formation of BCC, which increases the hardness and wear resistance [19]. Therefore, the hardness value is quite high because of the BCC structure, which possesses a higher hardness than FCC structures [1]. It was reported that the alloy $\text{Al}_2\text{CrFeCoCuTiNi}_x$ has a surface microhardness about 1102HV, which is 4 times higher than that of Q235 steel. The reason is the differences in the atomic radii of the elements, which result in distortion in the lattice, which in turn enhances the strengthening by solid solution effects [20]. With the increase of the Ni and Al contents, the hardness tended to increase. The reason is that the microhardness of FCC crystal structure is lower than BCC crystal structure. With the increase of Ni and Al contents, the content of BCC crystal structure increases in the alloys, so the hardness increased [20], [21].

Alloy 2:

For Alloy 2 $\text{CoCrFeNiAl}_{0.25}\text{Ti}_{0.75}$ high entropy alloy, as mentioned in the previous section, the crystal structure consists of BCC and FCC along with intermetallic compounds, which gives the alloy very high hardness averaged to be about 866 ± 22 as it can be seen from the Vickers hardness profile in Figure 6. However, it is so hard that it possesses brittle structure due to the ordering of BCC phases [16].

Table 4 lists the atomic radii for the element utilized in casting Alloys 2 and 3. The table states that Ni, Cu, Cr, Co, and Fe possess similar atomic sizes ranging between 1.25 to 1.27 Å. In addition, it shows that Al and Ti have similar atomic radii as well, which are 1.46 and 1.43 Å, respectively. Hence, the alloys have two levels of sizes. The ones with small sizes can be treated as solvents, whereas the others with larger sizes can be treated as solutes [22].

Table 4 Atomic radii of the elements employed in the Alloys 1 and 2 [23].

element	Ti	Fe	Co	Cr	Cu	Al	Ni
Atomic radius(Å)	1.46	1.26	1.25	1.27	1.24	1.43	1.24

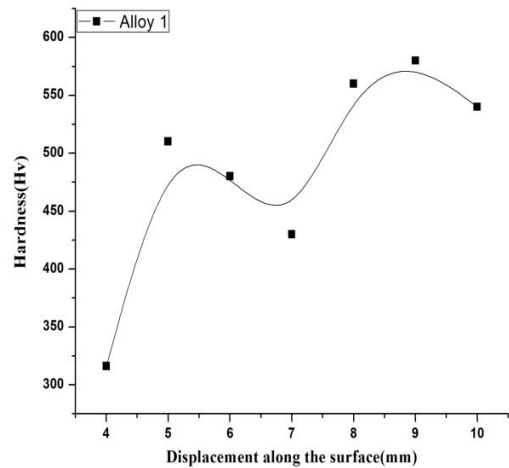


Figure 5. Vickers microhardness profile along the surface of Alloy 1 $\text{Co}_{0.5}\text{CrCu}_{0.5}\text{FeNi}_{1.5}\text{AlTi}_{0.4}$

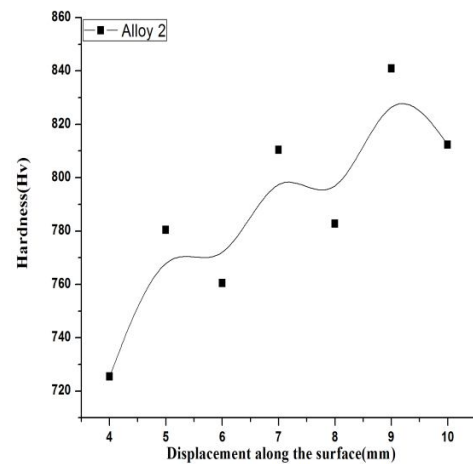


Figure 6. Vickers microhardness profile along the surface of Alloy 2 $\text{CoCrFeNiAl}_{0.25}\text{Ti}_{0.75}$

Optical microscopy

- Optical images show fine microstructure.
- Homogenous structures were obtained.
- No significantly observable porosity

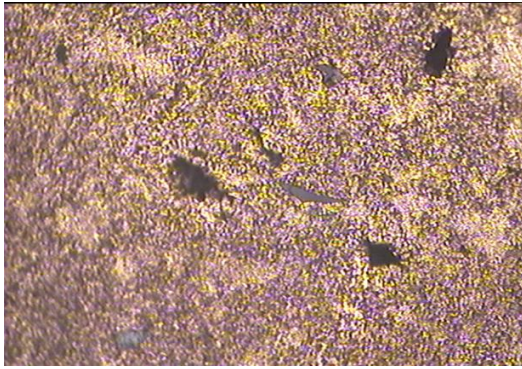


Figure 7 : Optical Images of Sintered Samples at 100x Magnification of alloy 1

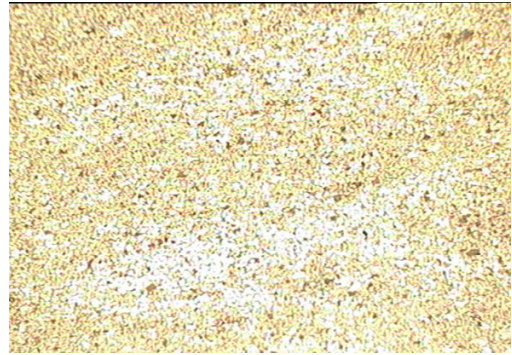


Figure 10 : Optical Images of Sintered Samples at 4x Magnification of alloy 2

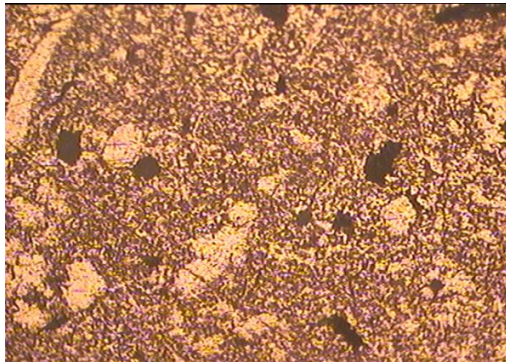


Figure 8 : Optical Images of Sintered Samples at 100x Magnification of alloy 2

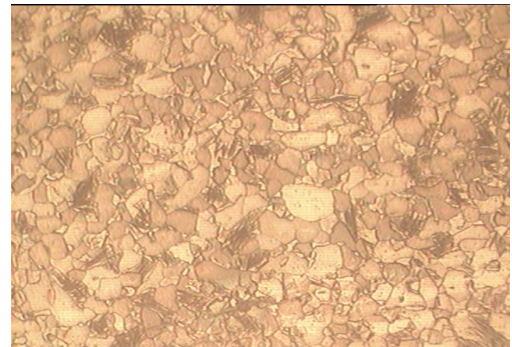


Figure 11 : Optical Images of Sintered Samples at 6x Magnification of alloy 1

This result showing that microstructure obtained from these both alloy have fine grain structure and almost zero porosity. from the result , it is clear that structure obtained from this experiment is homogenous. Obviously, structure should be homogenous as it is sintered for several hours of time. Due to sintering , it becomes densify , usually densification is the one of main purpose of sintering that results the good structure as well as excellent mechanical properties.

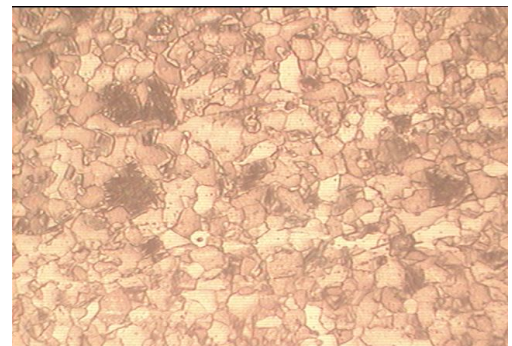


Figure 12 : Optical Images of Sintered Samples at 6x Magnification of alloy 2



Figure 9: Optical Images of Sintered Samples at 4x Magnification of alloy 1

Wear Analysis

From the figures it can be noticed, when cross-sectional area and depth of the wear track are large, the wear factor/rate will be higher. The lower wear rate in units of $\text{mm}^3/\text{N}\cdot\text{m}$, gives an indication of larger wear resistance. Also, note that as in the case of μ values, the wear rates are also system dependent, e.g. depend on counterface ball material, normal load, sliding speed, etc. Furthermore, the wear rates reported below are relative in that there is Si3N4 ball wear that transfers to the wear track thus biasing the wear rates. Therefore, the wear rates are likely a lot higher than reported

below due to this positive wear in the track. However, for comparisons between the 6 alloys, the wear rate values are still important.

Alloys 1 and 2

The wear rates of samples 1 and 2 are 2.73×10^{-8} and 3.93×10^{-8} , respectively. The average hardness values are 465.8 and 755.55 HV, respectively. They are the harder alloys, and thus exhibit lower wear. However as mentioned above, Alloy 2 is very brittle with assumed low fracture toughness. Tang et al. [27] reported that nitrated $Al_{0.5}CoCrCuFeNi$ alloy exhibited a higher friction coefficient of about 0.9 and lower wear rate of 3.69×10^{-5} . whereas, the unnitrated $Al_{0.5}CoCrCuFeNi$ alloy exhibited a lower friction coefficient of about 0.6 with higher wear rate of 6.38×10^{-4} . They attributed that to the surface hardness of the nitrated alloy of about 1300 HV, which is much higher than that 890 HV of the unnitrated one, which increases frictional stresses.

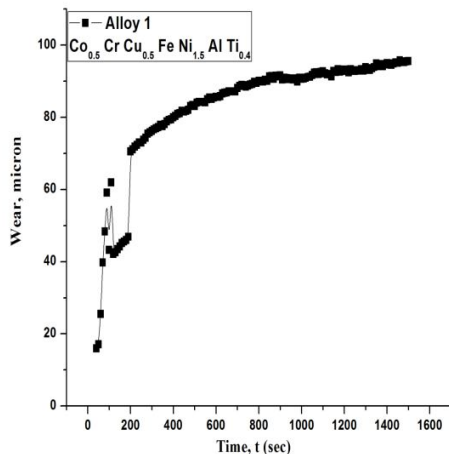


Figure 13 : wear vs time of Sintered Samples of alloy 1

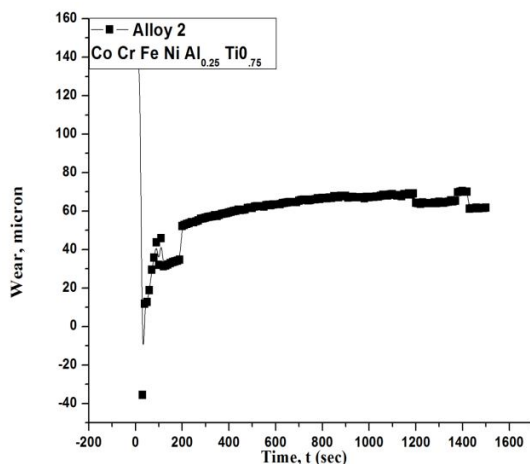


Figure 14 : wear vs time of Sintered Samples of alloy 2

In alloy 1 there are more wear than alloy 2 because of composition variation. Alloy 2 have six components and alloy 1 have seven component , as copper is absent in alloy 2, that's why composition variation in alloy 2 due to absence of Cu shows less wear as compare to alloy 1.

As copper shows face centered cubic structure with ductile and malleable behavior, hence it shows more wear in composition 1 as compare to composition 2. By hardness test it is clear that both alloys have high value of hardness and both are more wear resistant. but alloy 2 is more wear resistant as compare to alloy 1.

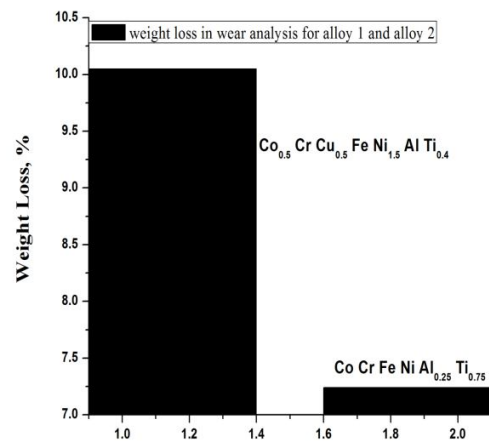


Figure 15 : percentage of weight loss in wear analysis of Sintered Samples of alloy 1 and alloy 2

V. CONCLUSION

Wear is a vital phenomenon in many industrial and engineering applications and machinery. Most available literature on friction and wear behavior of HEAs is very limited and none exists at elevated temperatures. Therefore, in the present work an attempt has been made to study the sliding wear properties of the two high entropy alloys at room temperature. In addition, mechanical hardness was measured as well. Moreover, fundamental mechanisms responsible for such behavior were determined by using Scanning Electron Microscopy (SEM), X-Ray Diffraction, and optical; spectroscopy. The evaluation of wear mechanisms was introduced in terms of microstructural evolution of the sliding surfaces. Combinations of wear mechanisms were found to take place between the sliding surfaces of both alloys used in this study. Moreover, the basic fundamentals of the characterization techniques employed to determine the tribological, mechanical, and morphological of the high entropy alloys and wear scars are discussed as well.

REFERENCES

- [1] Y. Zhang, T. T. Zuo, Z. Tang, M. C. Gao, K. A. Dahmen, P. K. Liaw, and Z. P. Lu, "Microstructures and properties of high-entropy alloys," *Prog. Mater. Sci.*, vol. 61, no. October 2013, pp. 1–93, 2014.
- [2] M.-H. Tsai, H. Yuan, G. Cheng, W. Xu, K.-Y. Tsai, C.-W. Tsai, W. W. Jian, C.-C. Juan, W.-J. Shen, M.-H. Chuang, J.-W. Yeh, and Y. T. Zhu, "Morphology, structure and composition of precipitates in Al 0.3 CoCrCu 0.5 FeNi high-entropy alloy," *Intermetallics*, vol. 32, pp. 329–336, 2013.
- [3] Z. Liu, S. Guo, X. Liu, J. Ye, Y. Yang, X. L. Wang, L. Yang, K. An, and C. T. Liu, "Micromechanical characterization of casting-induced inhomogeneity in an Al_{0.8}CoCrCuFeNi high-entropy alloy," *Scr. Mater.*, vol. 64, no. 9, pp. 868–871, 2011.
- [4] J. K. Lancaster, "Fundamentals of wear," *Tribol. Int.*, vol. 22, no. 4, pp. 301–302, 1989.
- [5] T. W. Scharf, "Tribological Improvements of carbon-carbon composites by infiltration of atomic layer deposited lubricious nanostructured ceramic oxides.," 2011.
- [6] J. F. Archard and W. Hirst, "The Wear of Metals under Unlubricated Conditions," *Proc. Roy. Soc. L.*, vol. A236, pp. 397–410, 1956.
- [7] O. O. Tinubu and B. Sc, "Effect of Friction Stir Processing on the Wear Behavior of Titanium (Ti-1Al-8V- 5Fe) and Stainless Steel (A-286) Alloys," 2015.
- [8] B. Cantor, *High-Entropy Alloys*. 2011.
- [9] Á. Vida, "Preparation and investigation of high entropy alloys," 2015.
- [10] E. Journal, "Recent progress in high-entropy alloys," no. December 2006, 2016.
- [11] J. Yeh, "Alloy Design Strategies and Future Trends in High-Entropy Alloys," vol. 65, no. 12, pp. 1759–1771, 2013.
- [12] W. F. Hosford, *Physical Metallurgy*. 2010.
- [13] M. De Graef, M. E. McHenry, and V. Keppens, "Structure of materials: An introduction to crystallography, diffraction, and symmetry," *The Journal of the Acoustical Society of America*, vol. 124, no. 3. p. 1385, 2008.
- [14] J. Yeh, "Alloy Design Strategies and Future Trends in High-Entropy Alloys," vol. 65, no. 12, pp. 1759–1771, 2013.
- [15] W. F. Hosford, *Physical Metallurgy*. 2010.
- [16] M. De Graef, M. E. McHenry, and V. Keppens, "Structure of materials: An introduction to crystallography, diffraction, and symmetry," *The Journal of the Acoustical Society of America*, vol. 124, no. 3. p. 1385, 2008.
- [17] D. A. Porter and K. E. Easterling, "phase transformations in metals and alloys," p. 154.
- [18] J. W. Yeh, "Alloy design strategies and future trends in high-entropy alloys," *Jom*, vol. 65, no. 12, pp. 1759–1771, 2013.
- [19] W. R. Wang, W. L. Wang, and J. W. Yeh, "Phases, microstructure and mechanical properties of Al_xCoCrFeNi high-entropy alloys at elevated temperatures," *J. Alloys Compd.*, vol. 589, pp. 143–152, 2014.
- [20] S. Guo, C. Ng, J. Lu, and C. T. Liu, "Effect of valence electron concentration on stability of fcc or bcc phase in high entropy alloys," *J. Appl. Phys.*, vol. 109, no. 10, 2011.
- [21] T. B. Massalski, "Comments Concerning Some Features of Phase Diagrams and Phase Transformations," *Mater. Trans.*, vol. 49, no. 5, pp. 192–201, 2010.
- [22] S. G. Ma, S. F. Zhang, M. C. Gao, P. K. Liaw, and Y. Zhang, "A successful synthesis of the CoCrFeNiAl_{0.3} single-crystal, high-entropy alloy by Bridgman solidification," *Jom*, vol. 65, no. 12, pp. 1751–1758, 2013.
- [23] X. Ye, M. Ma, W. Liu, L. Li, M. Zhong, Y. Liu, and Q. Wu, "Synthesis and Characterization of High-Entropy Alloy AlFeCoNiCuCr by Laser Cladding," *Adv. Mater. Sci. Eng.*, vol. 2011, pp. 1–7, 2011.
- [24] T. G. Novak, H. D. Vora, R. S. Mishra, M. L. Young, and N. B. Dahotre, "Synthesis of Al_{0.5}CoCrCuFeNi and Al_{0.5}CoCrFeMnNi High-Entropy Alloys by Laser Melting," *Metall. Mater. Trans. B Process Metall. Mater. Process. Sci.*, vol. 45, no. 5, pp. 1603–1607, 2014.
- [25] structure and composition of precipitates in Al 0.3 CoCrCu 0.5 FeNi high-entropy alloy," *Intermetallics*, vol. 32, pp. 329–336, 2013
- [26] Y. L. Chen, Y. H. Hu, C. W. Tsai, J. W. Yeh, S. K. Chen, and S. Y. Chang, "Structural evolution during mechanical milling and subsequent annealing of Cu-Ni-Al-Co-Cr-Fe-Ti alloys," *Mater. Chem. Phys.*, vol. 118, no. 2–3, pp. 354–361, 2009.
- [27] K. Zhang and Z. Fu, "Effects of annealing treatment on phase composition and microstructure of CoCrFeNiTiAl_x high-entropy alloys," *Intermetallics*, vol. 22, pp. 24–32, 2012.
- [28] F. Zhang, C. Zhang, S. L. Chen, J. Zhu, W. S. Cao, and U. R. Kattner, "An understanding of high entropy alloys from phase diagram calculations," *Calphad Comput. Coupling Phase Diagrams Thermochem.*, vol. 45, pp. 1–10, 2014.
- [29] T. T. Shun, C. H. Hung, and C. F. Lee, "Formation of ordered/disordered nanoparticles in FCC high entropy

- alloys,” *J. Alloys Compd.*, vol. 493, no. 1–2, pp. 105–109, 2010.
- [30] X. D. Xu, P. Liu, S. Guo, A. Hirata, T. Fujita, T. G. Nieh, C. T. Liu, and M. W. Chen, “Nanoscale phase separation in a fcc-based CoCrCuFeNiAl_{0.5} high-entropy alloy,” *Acta Mater.*, vol. 84, pp. 145–152, 2015.
- [31] X.-W. Qiu and C.-G. Liu, “Microstructure and properties of Al₂CrFeCoCuTiNi_x high-entropy alloys prepared by laser cladding,” *J. Alloys Compd.*, vol. 553, pp. 216–220, 2013.